PROF. SUJONG JEONG (Orcid ID : 0000-0003-4586-4534)

MR. HOONYOUNG PARK (Orcid ID : 0000-0002-7856-5218)

DR. DANICA LOMBARDOZZI (Orcid ID : 0000-0003-3557-7929)

DR. VANESSA HAVERD (Orcid ID : 0000-0003-4359-5895)

DR. ATUL JAIN (Orcid ID : 0000-0002-4051-3228)

DR. SÖNKE ZAEHLE (Orcid ID : 0000-0001-5602-7956)

DR. ETSUSHI KATO (Orcid ID : 0000-0001-8814-804X)

Enhanced regional terrestrial carbon uptake over Korea revealed by atmospheric CO$_2$ measurements from 1999 to 2017

Running head: Terrestrial carbon cycle from atmosphere

Jeongmin Yun[1], Su-Jong Jeong[2*], Chang-Hoi Ho[1], Hoonyoung Park[2], Junjie Liu[3], Haeyoung Lee[4], Stephen Sitch[5], Pierre Friedlingstein[6], Sebastian Lienert[7], Danica Lombardozzi[8], Vanessa Haverd[9], Atual Jain[10], Sönke Zaehle[11], Etsushi Kato[12], Hanqin Tian[13], Nicolas Vuichard[14], Andy Wiltshire[15], Ning Zeng[16]

[1]School of Earth and Environmental Sciences, Seoul National University, Seoul, Republic of Korea

[2]Department of Environmental Planning, Graduate School of Environmental Studies, Seoul National University, Seoul, Republic of Korea

[3]Jet Propulsion Laboratory, California institute of Technology, Pasadena, CA 91109, USA

[4]Environmental Meteorology Research Division, National Institute of Meteorological Sciences, Jeju, 63568, Republic of Korea

[5]College of Life and Environmental Sciences, University of Exeter, Exeter EX4 4RJ, UK

[6]College of Engineering, Mathematics and Physical Sciences, University of Exeter, Exeter 4QF, UK

[7]Climate and Environmental Physics, Physics Institute and Oeschger Centre for Climate Change Research, University of Bern, Bern, Switzerland

[8]National Center for Atmospheric Research, Boulder, Climate and Global Dynamics, Terrestrial Sciences Section, Boulder, CO 80305, USA

[9]CSIRO Oceans and Atmosphere, Canberra, ACT 2601, Australia

[10]Department of Atmospheric Sciences, University of Illinois, Urbana, IL, USA

[11]Biogeochemical Integration Department, Max Planck Institute for Biogeochemistry, 07745 Jena, Germany

[12]Research & Development Division, Institute of Applied Energy (IAE), Tokyo 105-0003, Japan

[13]School of Forestry and Wildlife Sciences, Auburn University, 602 Duncan Drive, Auburn, AL 36849, USA

[14]Laboratoire des Sciences du Climat et de l'Environnement, Institut Pierre-Simon Laplace, CEA-CNRS-UVSQ, CE Orme des Merisiers, 91191 Gif-sur-Yvette CEDEX, France

[15]Met Office Hadley Centre, FitzRoy Road, Exeter EX1 3PB, UK

[16]Department of Atmospheric and Oceanic Science and Earth System Science, Interdisciplinary Center, University of Maryland, College Park, Maryland, USA

Global Change Biology

(Primary Research Article)

*Corresponding author: Prof. Su-Jong Jeong (+82-2-880-5664; sujong@snu.ac.kr)

Abstract

Understanding changes in terrestrial carbon balance is important to improve our knowledge of the regional carbon cycle and climate change. However, evaluating regional changes in the terrestrial carbon balance is challenging due to the lack of surface flux measurements. This study reveals that the terrestrial carbon uptake over the Republic of Korea has been enhanced from 1999 to 2017 by analyzing long-term atmospheric CO_2 concentration measurements at Anmyeondo Station (36.53°N, 126.32°E) located in the western coast. The influence of terrestrial carbon flux on atmospheric CO_2 concentrations (ΔCO_2) is estimated from the difference of CO_2 concentrations that were influenced by the land sector (through easterly winds) and the Yellow Sea sector (through westerly winds). We find a significant trend in ΔCO_2 of -4.75 ppmv decade^{-1} ($p < 0.05$) during the vegetation growing season (May through October), suggesting that the regional terrestrial carbon uptake has increased relative to the surrounding ocean areas. Combined analysis with satellite measured normalized difference vegetation index and gross primary production shows that the enhanced carbon uptake is associated with significant nationwide increases in vegetation and its production. Process-based terrestrial model and inverse model simulations estimate that regional terrestrial carbon uptake increases by up to 9.9 and 4.2 Tg C decade^{-1}, accounting for 13.4 and 5.7% of annual domestic carbon emissions averaged for the study period, respectively. Atmospheric chemical transport model simulations indicate that the enhanced terrestrial carbon sink is the primary reason for the observed ΔCO_2 trend rather than anthropogenic emissions and atmospheric circulation changes. Our results highlight the fact that atmospheric CO_2 measurements could open up the possibility of detecting regional changes in the terrestrial carbon cycle even where anthropogenic emissions are not negligible.

Introduction

Atmospheric CO_2 concentration has risen from 278 parts per million by volume (ppmv) in pre-industrial times (1750) (Joos & Spahni, 2008) to 405 ppmv in 2017 (Dlugokencky & Tans, 2019) owing to anthropogenic carbon emissions. Elevated atmospheric CO_2 increases the global mean temperature, which contributes to changes in the magnitudes and intensities of extreme weather events such as heat waves, droughts, and heavy rainfall (Min, Zhang, Zwiers, & Hegerl, 2011; IPCC, 2014; Seneviratne, Donat, Pitman, Knutti, & Wilby, 2016). Thus, a clear understanding of the carbon cycle is critical for the recognition of contemporary climate change as well as future climate projections. The Global Carbon Project (GCP) (http://www.globalcarbonproject.org/), an international research project, estimates the annual global carbon budget using the latest models and observations to identify processes contributing to atmospheric CO_2 changes (Le Quéré et al., 2018). As a part of the GCP, the REgional Carbon Cycle Assessment and Processes project (RECCAP; Canadell et al., 2011) quantifies carbon fluxes on subcontinental scales. GCP estimated an imbalance of approximately 5% in the recent global carbon budget (Le Quéré et al., 2018). In line with GCP estimations, RECCAP highlighted significant uncertainties in the regional carbon budget (Haverd et al., 2013; Patra et al., 2013; Piao et al., 2013; Sitch et al., 2015; Thompson et al., 2016), implying limitations in our knowledge about spatiotemporal variations in the regional carbon cycle. Therefore, comprehensive analysis and assessment of the regional carbon cycle, including anthropogenic carbon emissions and land surface carbon balance, could reduce uncertainties in the global carbon cycle.

Terrestrial ecosystems alleviated the increasing atmospheric CO_2 by absorbing approximately one third of emitted anthropogenic carbon from fossil fuel combustion and land use change in 2017 (Le Quéré et al., 2018). Due to the high capability for carbon assimilation, terrestrial ecosystems are considered one of the main components of the regional carbon cycle. However, lack of relevant information on its spatial distribution and temporal variation has made it difficult to assess changes in the terrestrial carbon sink. To estimate the changes, previous studies have utilized process-based land surface models (Piao et al., 2011; Cui et al., 2014; Lee et al., 2014; Yue, Unger, & Zheng, 2015), the inverse modeling approach (Enting & Mansbridge, 1989; Gurney et al., 2003; Nassar et al., 2011; Liu et al., 2014), forest inventories (Choi, Lee, & Chang, 2002; Pan et al., 2011; Jeong et al., 2013; Fang et al., 2014), and eddy covariance tower

measurements (Piao et al., 2008; Dragoni et al., 2011; Keenan et al., 2014; Yun & Chun, 2018). Process-based models are useful for estimating responses of terrestrial ecosystems to environmental change on regional to global scales, but they have inherent uncertainties. While inverse modeling frameworks help to reduce the uncertainties in flux estimation by using atmospheric CO_2 measurements, the inversion results are highly sensitive to the distribution of observation sites (Bruhwiler, Michalak, and Tans, 2011) and physical parameterizations in transport models (Patra et al., 2008; Peylin et al., 2013). National forest inventories provide reliable quantitative information on forest biomass changes, but parameter uncertainties also occur when estimating forest carbon stock. Flux tower measurements directly observe terrestrial carbon exchange with the atmosphere; however, the number of measurement sites is insufficient for detecting regional-scale changes due to its large spatial heterogeneity. Recently, new approaches have been introduced to overcome the limitations of ground-based observations and models (Parazoo et al., 2016; Commane et al., 2017, Jeong et al., 2018). For example, the study by Jeong et al. (2018) showed that the ecosystem in the northern Alaska region has become a carbon source during autumn by separating regional influence on atmospheric CO_2 at Barrow from the background. As such, previous studies have shown that long-term atmospheric CO_2 observations could help us to evaluate the role of specific components, such as terrestrial ecosystems, in determining atmospheric CO_2 concentrations in data-limited environments.

The Republic of Korea (Korea), located in East Asia, has been experiencing rapid economic development and land-use change over recent decades. The gross domestic product has more than tripled between 1999 and 2017 (World Bank, 2018) because of accelerated industrialization and urbanization since the 1970s. With this economic growth, there is an associated increase in energy consumption that is predominantly supplied by fossil fuels, making Korea the 9th largest fossil fuel CO_2 emitter in the world in 2017 (168 Tg C year^{-1}; Global Carbon Project, 2018). Thus, Korea is likely a hot spot of carbon emissions. In contrast to the large emissions, there is the carbon sink across the country, which has changed considerably over the recent decades. A national reforestation and forest management plan was implemented in 1973, and sustained forest management by the national forestry department and the local governments has increased the forest volume in Korea from 60.3 m^3 ha^{-1} in 1999 to 146.0 m^3 ha^{-1} in 2015 (Korea Forest Service, 2018). The managed young forests, occupying around 65% of the country, had the highest carbon

sequestration rate over East Asia of 5–12 Tg C year^{-1} in the 1990s and 2000s (Choi et al., 2002; Li, Yi, Son, Jin, & Han, 2010) and have potentially offset 8.9% of the domestic anthropogenic emissions from the 1970s to 2000s (Fang et al., 2014). Furthermore, a longer vegetation growing season related to regional warming could contribute to enhanced carbon sequestration over Korea (Jeong et al., 2013). Therefore, assessing the role of terrestrial ecosystem change in the regional carbon cycle is critical to understanding the carbon cycle dynamics.

Continuous monitoring of atmospheric CO_2 concentrations has been carried out in Korea at Anmyeondo (AMY) since 1999. The AMY site is located on the western tip of the Korean Peninsula, which is surrounded by the ocean on three sides and has the advantage of being able to monitor variations in atmospheric CO_2 both within and outside the mainland. Using the long-term measurements at the AMY site, we assessed the possibility of using atmospheric CO_2 measurements to understand the terrestrial carbon cycle at a regional scale (i.e. Korea). First, we estimated the influence of regional land-surface on atmospheric CO_2 from the difference between CO_2 concentrations measured when wind blows from the land sector and from the Yellow Sea sector, which can be considered a proxy for the net ecosystem exchange, as in Jeong et al. (2018). To further explain the observed regional changes in atmospheric CO_2, we identified vegetation and terrestrial carbon flux changes using satellite measurement datasets and model simulation results, respectively. The influences of changes in regional land–surface carbon fluxes as well as atmospheric transport on the CO_2 concentration were also evaluated through chemical transport model simulations. Multiple lines of evidence provide reliable information on changes in the terrestrial carbon cycle over Korea during the last two decades in this study.

Materials and methods

This study combines both observational analysis and model simulations to investigate changes in the terrestrial carbon cycle over Korea in the last two decades. We first detected the signal of changes in regional land–surface carbon fluxes from the difference between CO_2 concentrations measured at the AMY Station when wind blows from the land sector and from the Yellow Sea sector (ΔCO_2). We hypothesized that the observed ΔCO_2 trend could be associated with changes in the regional terrestrial carbon fluxes. To support our hypothesis, we identified changes in

vegetation and terrestrial carbon fluxes in the region. The changes in vegetation and its production were investigated using the GIMMS and MODIS NDVI datasets and MODIS GPP dataset, respectively. The changes in terrestrial carbon fluxes were estimated using the TRENDY model simulation results and the CT2017 dataset. GEOS-Chem model simulations were also conducted to evaluate the influences of changes in regional terrestrial carbon fluxes as well as fossil fuel carbon emissions and atmospheric circulation on the CO_2 concentration over Korea.

Atmospheric CO_2 observation

The Anmyeondo Observatory (36.53°N, 126.32°E) is one of 112 World Meteorological Organization (WMO) Global Atmosphere Watch (GAW) regional stations (Figure 1). The Korea Meteorological Administration (KMA) has continuously measured atmospheric CO_2 concentrations at the site from a 40 m tower (47 m above sea level) since January 1999 (Cho, Kim, & Yoo, 2007; Lee, Han, Ryoo, Lee, & Lee, 2019). The collected data are managed by the World Data Centre for Greenhouse Gases (WDCGG). We used hourly CO_2 concentration data from January 1999 to October 2017 that were calibrated through quality control processes reported by Lee et al. (2019). The reliability of the hourly data was evaluated by comparison with flask-air samples collected weekly at the AMY Station (Lee et al., 2019).

Because long-term CO_2 measurements have been performed at only one station in Korea, we sampled hourly CO_2 concentration data based on wind direction and built two different monthly datasets, which likely represent land-influenced CO_2 concentration (CO_2^{land}) and background CO_2 concentration for the CO_2^{land} ($CO_2^{YellowSea}$), respectively. Due to absence of local wind data, we used hourly wind data from the Automatic Synoptic Observation System at the Seosan Station, which is the wind measurement site nearest to the AMY Station (around 30 km). To reduce the effect of local CO_2 sources and expand the area of influence, we only considered the hourly CO_2 data with wind speeds exceeding 3 m s^{-1} during the daytime (from 12:00 p.m. to 17:00 p.m.) when vertical mixing is active. Our main findings are identical when the threshold is between 2.5 and 3.5 m s^{-1}. Taking into account the coastline layout, CO_2^{land} is defined as observations made when the wind direction was between 45° and 135° (land sector). $CO_2^{YellowSea}$ is defined as observations made when the wind direction was between 225° and 315° (Yellow Sea sector). Using wider

ranges of wind direction did not alter our results, but we aimed to discriminate between CO_2^{land} and $CO_2^{YellowSea}$. The separated CO_2^{land} and $CO_2^{YellowSea}$ were smoothed by the curve-fitting method of Thoning et al. (1989) and aggregated into monthly values. Finally, the difference between the monthly CO_2^{land} and $CO_2^{YellowSea}$ ($\Delta CO_2 = CO_2^{land}$ minus $CO_2^{YellowSea}$) was treated as a proxy for the atmospheric signal for regional land–surface carbon fluxes over Korea at a monthly scale. This approach has been applied to determine the changes in regional land-surface CH_4 and CO_2 exchange (Sweeney et al., 2016; Commane et al., 2017; Jeong et al., 2018).

The KMA has also been monitoring atmospheric CO_2 concentrations at Ulleungdo (ULD; 37.48°N, 130.90°E) from a 10 m tower (221 m above sea level) with the same measurement system of Anmyeondo (AMY) Station since 2014 after two years of test operation (Lee et al., 2019). The ULD Station is located at Ulleungdo (72 km^2), approximately 155 km east from the mainland (Figure 1), and data from this site represents the atmospheric CO_2 flowing into the mainland from the East Sea. Hourly CO_2 concentrations at the ULD Station were compared with the CO_2^{land} to validate whether the variations of CO_2^{land} are mainly attributed to the regional land–surface CO_2 fluxes or the air coming from the East Sea. The hourly ULD CO_2 concentration data were smoothed by the curve-fitting method of Thoning et al. (1989) and aggregated into monthly values from January 2014 to October 2017.

Back-trajectory analysis

To verify our classification between CO_2^{land} and $CO_2^{YellowSea}$ based on locally measured wind data, we investigated inflow direction of air masses for winds from the land and Yellow Sea sectors using a back-trajectory model. We used the National Oceanic and Atmospheric Administration (NOAA) HYbrid Single-Particle Lagrangian Integrated (HYSPLIT, version 4; Stein et al., 2015) model to calculate 48-h back-trajectories of air masses arriving at the AMY Station. The trajectories started 500 m above sea level, which are within the daytime mixing layer height. Altering the initial altitude level from 500 m to 1000 m did not change results in this study. The National Centers for Environmental Prediction/National Center for Atmospheric Research (NCEP/NCAR) reanalysis meteorological dataset with a 6-h interval and spatial resolution of 2.5° was used as the model input.

Trajectory densities of the air masses were generated at a 0.5° × 0.5° spatial resolution to investigate the overall spatial patterns of the trajectories for each case; we calculated the percentage of the number of trajectories passing through each grid cell among the total number of back-trajectories. The percentage decreases farther away from the station where a value of 100% appears, which indicates that all trajectories pass the area (Figure 2). Trajectory distributions of the air masses for wind from the Yellow Sea sector and from the land sector explicitly differ. To gather quantitative information, we set a domain centered at the station (35.5–37.5°N, 125.3–127.3°E; boxed area in Figure 2a) and noted the direction from which the air masses arrived at the domain. 88.3% of the air mass for wind from the Yellow Sea sector enters the domain from the ocean side (Figure 2a). The northwestern airflow, which crosses the west coast of the Korean Peninsula, is dominant. Conversely, 82.9% of the air mass for wind from the land sector enters the domain from the landside (Figure 2b). The main airflows arrive at the station directly from the eastern Korean Peninsula. The remaining 17.1% of the air mass enters the domain from the ocean side, especially northwest of the station. The mismatched air mass contributes to shifting the median of back-trajectories in the east coast of the Korean Peninsula toward the northwest between 36 and 48 hours prior. These trajectory patterns indicate that our wind direction-based classification is reasonable for separating the air mass into two groups: inflow from outside and inflow from inside the Korean Peninsula ($CO_2^{YellowSea}$ and CO_2^{land}).

Satellite-measured NDVI dataset

Remote sensing provides continuous observational data over vast areas. Satellite-measured normalized difference vegetation index (NDVI) datasets have been widely used to detect variations in vegetation growth (Jeong, Ho, & Jeong, 2009; Jeong et al., 2013; Zhang, Song, Band, Sun, & Li, 2017). Here, we used two different satellite-measured NDVI datasets, the Global Inventory Monitoring and Modeling System (GIMMS) 3g NDVI and Moderate Resolution Imaging Spectroradiometer (MODIS) NDVI, to gather more reliable information of the changes in vegetation over Korea during the last two decades.

The third generation of the GIMMS NDVI dataset was produced from advanced very high-resolution radiometers (AVHRRs) on the polar-orbiting meteorological satellites of NOAA and European organizations for the exploitation of meteorological satellites (Pinzon & Tucker, 2014). The dataset was calibrated using the Bayesian method and other satellite-measured NDVI data derived from the sea-viewing wide field-of-view sensor. The reported accuracy of the data is within ± 0.005 (Pinzon & Tucker, 2014). The GIMMS NDVI dataset covers the period from July 1981 to December 2015 with a 1/12 degree of spatial resolution and 15-day intervals. The data for the period overlapping with the AMY CO_2 data-collection period were used for the current study (from 1999 to 2015).

The MODIS NDVI dataset from MOD13C1 (Version 6) products was derived from MODIS Terra images (Didan, 2015). The MOD13C1 dataset is spatially aggregated from 1 km of cloud-free MOD13A2 data to a 0.05° geographic climate modeling grid with 16-day intervals and covers the period from February 2000 to the present. Reliability of the MODIS NDVI dataset was evaluated by comparisons with other existing satellite-measured NDVI data, and its accuracy is within ± 0.025 (MODIS Land Team, 2018). The data for the period overlapping with the AMY CO_2 data collection period was used for the current study (from 2000 to 2017).

MODIS GPP

The MODIS gross primary production (GPP) dataset from MOD17A2H (Version 6) products from MODIS Aqua and Terra images were used to estimate the changes in GPP in Korea from 2000 to 2017 (Running and Zhao, 2015). The algorithm based on light-use efficiency concepts was applied to generate the GPP dataset from the meteorological field of the Global Modeling and Assimilation Office supported by the National Aeronautics and Space Administration and satellite-derived fraction of photosynthetically active radiation from MOD15 (Running and Zhao, 2015). The MOD17A2H dataset is a cumulative 8-day composite of values with 500 m spatial resolution and covers the period from February 2000 to the present. The MODIS GPP dataset was spatially aggregated from 500 m to a 0.05° geographic climate modeling grid to match the spatial resolution of MODIS NDVI for the current study.

TRENDY models

We used monthly averaged carbon fluxes (GPP, Ra; autotrophic respiration, Rh; heterotrophic respiration, and NBP; net biome production) simulated by 11 dynamic global vegetation models from the TRENDY project version 6 (simulation S3; Sitch et al., 2015) to estimate changes in terrestrial carbon fluxes over Korea from 2000 to 2016. The list of models used is as follows: CABLE (Haverd et al., 2018), CLM4.5 (Oleson et al., 2013), DLEM (Tian et al., 2015), ISAM (Jain, Meiyappan, Song, & House, 2013), LPJ (Sitch et al., 2003), LPX-Bern (Stocker, Feissli, Strassmann, Spahni, & Joos, 2014), OCN (Zaehle, Friedlingstein, & Friend, 2010), ORCHIDEE (Krinner et al., 2005), VEGAS (Zeng, Mariotti, & Wetzel, 2005), VISIT (Ito & Inatomi, 2012), and JULES (Clark et al., 2011). Models were forced by observed climate fields from the Climate Research Unit (CRU) dataset (CRU-TS 3.23 and 3.25) or CRU-National Centers for Environmental Prediction version 8 meteorological dataset, global atmospheric CO_2 concentration data from ice-cores and atmosphere measurements from NOAA Earth System Research Laboratory (ESRL) (Dlugokencky & Tans, 2019), and land use and land cover change data from the HYDE database (Hurtt et al., 2011). The model outputs from the TRENDY project have been applied in a number of studies to estimate the changes in terrestrial carbon balance and to understand the driving factors for the change at global as well as regional scales (Piao et al., 2012; Le Quéré et al., 2018).

GEOS-Chem model simulations

We used the Goddard Earth Observing System (GEOS)-Chem model, a global 3-D chemical transport model (CTM) for atmospheric compositions (Bey et al., 2001), to evaluate the influences of changes in the regional land–surface carbon fluxes and atmospheric transport on the CO_2 concentrations over Korea. We conducted GEOS-Chem CO_2 simulations, which ignore the chemical reactions of CO_2 but consider surface CO_2 fluxes to the atmosphere and transport of atmospheric CO_2. This version of the model has been widely used to investigate the response of atmospheric CO_2 to changes in fossil fuel emissions (Nassar et al., 2013) and terrestrial carbon fluxes (Barnes, Parazoo, Orbe, & Denning, 2016; Parazoo et al., 2016).

We used a nested-grid GEOS-Chem model (version 11.2) with the native $0.5° \times 0.667°$

horizontal resolution and 47 vertical layers from surface pressure to 0.01 hPa over East Asia (11°S–55°N, 70–150°E) (Wang, McElroy, Jacob, & Yantosca, 2004). Boundary conditions for the nested version of the model were provided hourly from the global GEOS-Chem simulations with 4° × 5° horizontal resolution. All model simulations were performed by using observed meteorological data and land-surface carbon flux datasets. We used the hourly meteorological data from the Modern-Era Retrospective analysis for Research and Applications version 2 (MERRA-2) reanalysis datasets with the same spatial resolutions as each simulation (Gelaro et al., 2017). The carbon flux datasets include terrestrial biospheric exchange, ocean exchange (Takahashi et al., 2009), emissions from fossil fuels, biomass burning (Randerson, Van Der Werf, Giglio, Collatz, & Kasibhatla, 2018), biofuel burning (Yevich & Logan, 2003), shipping, and aviation (Simone, Stettker, & Barrett, 2013). Among the carbon flux dataset, monthly terrestrial carbon fluxes and fossil fuel carbon emissions were taken from CarbonTracker outputs (CT2017; Peters et al., 2007) and the Open-source Data Inventory for Anthropogenic CO_2 (ODIAC) dataset (Oda & Maksyutov, 2011), respectively.

GEOS-Chem was spun up from 1990 to 1999 using the meteorological data and fossil fuel carbon emission data of 1990–1999 and the other surface CO_2 flux datasets fixed at their values in 2000. Starting from the model state in 2000, we performed a set of sensitivity simulations from 2000 to 2016 (Table 1). In simulation E1, all variables used are transient. In simulations E2, E3, and E4, one or both monthly terrestrial carbon fluxes and fossil fuel carbon emissions in 2000 are repeatedly prescribed over Korea (34–38°N, 126–130°E) during the entire simulation period; however, other conditions are identical to those of simulation E1. Simulation E5 is identical to simulation E3, but the carbon emissions in 2000 are prescribed over eastern China (20–40°N, 100–125°E and 40–50°N, 100–140°E) not Korea. From the differences between simulation E1 and simulations E2 and E3 (e.g. simulation E1 minus simulation E2), influences of the changes in regional terrestrial carbon flux and anthropogenic carbon emissions on atmospheric CO_2 in Korea were estimated, respectively. The possible influences of changes in transported atmospheric CO_2 from other regions were estimated in simulation E4. The effect of changes in anthropogenic carbon emissions in eastern China, which are expected to account for the largest portion of the transported CO_2, was estimated from the difference between simulations E1 and E5. The model bias related to the overestimation of the long-term trend in CO_2 concentrations was corrected by

comparing the AMY CO_2 concentration data. Simulated surface CO_2 concentrations were only used for analysis in the study.

In the case of terrestrial carbon fluxes, we conducted an additional set of model simulations using TRENDY model results. In simulation T1 (control simulation), monthly terrestrial carbon flux for a specific year are repeatedly prescribed during the entire simulation period; there are no annual changes in the seasonal variation of the terrestrial carbon flux. In simulations T2, T3, and T4 (sensitivity simulations), the monthly flux in Korea is set to linearly change from the fixed value by the average, maximum, and minimum trends of the estimated NBP in the TRENDY models during the entire simulation period. The range of influences of the estimated NBP changes on the CO_2 concentrations are obtained from the differences of simulations T2, T3, and T4 with simulation T1.

Results

The signal of regional land-surface carbon flux changes on atmospheric CO_2

Both time series of CO_2^{land} and $CO_2^{YellowSea}$ at the AMY Station show gradually increasing trends and clear seasonal variations, with the maximum in early spring and minimum in late summer from January 1999 to October 2017 (Figure 3a). However, the seasonal variability of CO_2^{land} is greater than that of $CO_2^{YellowSea}$. Compared with $CO_2^{YellowSea}$, annually averaged CO_2^{land} is lower by 1.9 ppmv on average during the growing season (from May to October) and higher by 3.6 ppmv on average during the non-growing season (from November to April) for the total study period (Figure 3b; black thick line). In recent years, notable decreases in annually averaged ΔCO_2 during the growing season appear from 0.5 ± 2.1 ppmv in 1999–2006 to -5.0 ± 2.2 ppmv in 2010–2017 (Figure 3b; bar). The annually averaged monthly ΔCO_2 in the two periods are out of each other's error ranges as represented by the 1σ in May, June, July, and September. For example, the annually averaged ΔCO_2 in May is 1.0 ± 3.0 ppmv in the first eight years and -4.8 ± 3.8 ppmv in the last eight years. The results suggest that the recent decreases in ΔCO_2 for the growing season are not considered as noise. A statistically significant trend of the ΔCO_2 is also observed for the growing season, on average, at -4.75 ppmv decade^{-1} ($p < 0.05$; Figure 3c); it

corresponds to an increase of 250% decade^{-1} of the magnitude of its climatological value since the climatological value is small. On the contrary, an increase in the ΔCO_2 is observed from November to March at 1.27 ppmv decade^{-1}, but this is not significant. The results suggest that the atmospheric CO_2 concentration over Korea rises slowly relative to the surrounding ocean regions during the growing season for the last two decades.

Changes in vegetation and terrestrial carbon fluxes

To understand the reasons for the observed negative ΔCO_2 trends during the growing season, we evaluated the changes in vegetation and terrestrial carbon fluxes over Korea for the last two decades. Korea, where two thirds of the country are forested (Korea Forest Service, 2018), has a climatological NDVI of 0.69 (GIMMS: 0.69, MODIS: 0.69; Figure 4a, b) and an accumulated GPP of 919 gC m^{-2} during the growing season (Figure 4c). Both two different satellite observe nationwide positive trends in NDVI (Figure 4a, b). For the growing season, the NDVI from GIMMS increases by 0.030 decade^{-1} over 92.1% of the region from 1999 to 2015; this accounts for a 4.3% decade^{-1} increase. Similarly, the NDVI from MODIS increases by 0.025 decade^{-1} over 93.7% of the entire study area from 2000 to 2017; this accounts for a 3.6% decade^{-1} increase. The increasing trends of NDVI from GIMMS and MODIS are significant at the 95% confidence level in 34.4% and 75.1% of the study area, respectively. In line with the observed nationwide vegetation greening, accumulated GPP from MODIS increases by 68.6 gC m^{-2} decade^{-1} over 93.9% of the entire study area during the growing season from 2000 to 2017; this accounts for a 7.5% decade^{-1} increase (Figure 4c). Some parts of central Korea show decreases or little changes in the GPP, but a significant increase in the GPP is observed in 45.1% of the analysis domain, especially over the southwestern part of Korea.

The TRENDY multi-model mean overestimates the climatological value of the area-averaged accumulated GPP over the study area during growing season as 1269 ± 277 gC m^{-2}, but it estimated an increase in GPP for the season by 54.8 ± 27.5 gC m^{-2} decade^{-1}, similar to the GPP from MODIS (61.4 gC m^{-2} decade^{-1}) for 2000–2016 (Figure 5a). Due to the relatively low increase in total respiration (36.0 ± 29.0 gC m^{-2} decade^{-1}) compared with the GPP, the net terrestrial carbon uptake (i.e. NBP) has been enhanced by 18.5 ± 24.0 gC m^{-2} decade^{-1} during the growing season

(Figure 5b, c), corresponding to a $14.8 \pm 19.2\%$ decade^{-1} increase of its climatological value (125 $\pm$ 105 gC m^{-2}). Even though large variations among the TRENDY models exist from -48.7 to 101.3 gC m^{-2} decade^{-1} (this accounts for 39.0% decade^{-1} decrease and 81.0% decade^{-1} increase), the NBP from the multi-model mean has the same sign with the trends of the biospheric carbon flux of 42.9 gC m^{-2} decade^{-1} from CT2017, corresponding to 45.5% decade^{-1} increase of its climatological value (94.2 gC m^{-2}). The estimated enhancement of terrestrial carbon uptake from TRENDY and CT2017 models accounts up to 13.4 and 5.7% of annual domestic carbon emissions averaged for the study period (141 Tg C year^{-1}; Global Carbon Project, 2018), respectively. Both models also estimate a relatively weak increasing trend of the carbon flux in July than adjacent months. This is due to the stagnant rain front, which blocks solar radiation and inhibits vegetation growth over Korea during the summer rainy season (Lee et al., 2017). These results derived from independent datasets and models suggest that the terrestrial carbon uptake in Korea has increased during the growing season due to the nationwide vegetation greening for the last two decades.

Influences of changes in regional land–surface carbon fluxes on atmospheric CO_2

We performed CTM simulations to implement the influences of model-estimated changes in regional terrestrial carbon fluxes on the atmospheric CO_2 in Korea from 2000 to 2016. The enhanced terrestrial carbon uptake estimated in both CT2017 and TRENDY multi-model mean consistently induce decreases in CO_2 concentrations in Korea during the growing season, distinct from the non-growing season (Figure 6a). In the case of the CT2017, CO_2 concentration decreases by 0.64 ppmv decade^{-1} during the growing season and shows little increase (0.06 ppmv decade^{-1}) during the non-growing season (Figure 6a; red line). The maximum decreasing trend appears in June at 1.25 ppmv decade^{-1}, as do the observed ΔCO_2 trend. In the case of the TRENDY models, CO_2 concentration decreases up to 1.37 ppmv decade^{-1} during the growing season, even though the multi-model mean estimated a relatively small decrease (0.24 ppmv decade^{-1}) than CT2017 (Figure 6a). A possible maximum decreasing trend of the CO_2 concentration is also exhibited in June at 2.39 ppmv decade^{-1}. The results suggest that the regional enhancement of terrestrial carbon uptake is the main reason for the observed negative trend in the ΔCO_2 during the growing season for the study period.

In addition to the biosphere fluxes, anthropogenic carbon emissions increased by 33 Tg C decade^{-1} in Korea for the analysis period. Seasonal differences in the monthly carbon emissions trends also appear; the trends of the non-growing season (2.9 Tg C month^{-1} decade^{-1}) are greater than those of the growing season (2.6 Tg C month^{-1} decade^{-1}) by 0.3 Tg C month^{-1} decade^{-1} on average; the difference accounts for around 11% of the annual mean trends. Our model estimates that the rise in domestic carbon emissions increases annual mean CO_2 concentrations in Korea by 1.11 ppmv decade^{-1} (Figure 6b). However, notable seasonal differences are not observed in the increasing trends; the seasonally averaged trends are 1.04 and 1.17 ppmv decade^{-1} during the growing season and non-growing season, respectively. The model simulation results suggest that domestic carbon emissions are not a main reason for the observed ΔCO_2 trends.

Influences of atmospheric transport changes on atmospheric CO_2 over Korea

Korea is located in the downstream area of China, the biggest CO_2 emitter in the world, and close to a strong summer uptake region (Siberia). Considering the geographical location, the influences of atmospheric transport changes on CO_2 concentrations over Korea are also evaluated through model simulations. Even without considering the land–surface carbon flux changes in Korea, annual mean CO_2 concentrations increased more than 21 ppmv decade^{-1} from 2000 to 2016 over East Asia. The largest increase is found in eastern China at more than 31 ppmv decade^{-1} and the increasing trend is weakened further away from the region (Figure 7a). The spatial distributions of the increasing trends are mostly associated with a steep rise of fossil fuel carbon emissions in eastern China at 1.4 Pg C decade^{-1} for the analysis period. The increasing carbon emissions raises CO_2 concentrations in the main source regions such as the north China plain, Beijing, and Shanghai by more than 13 ppmv decade^{-1}, as well as surrounding regions including Korea by more than 6 ppmv decade^{-1} (Figure 7b). We compared the influences of atmospheric transport change on the monthly trends of atmospheric CO_2 in the surrounding area (Yellow Sea) and in the Korean Peninsula (boxed area in Figure 8): Region1 (35–38°N, 123.0–126.0°E) and Region2 (35–38°N, 126.5–129.5°E).

The atmospheric transport changes raise the annual mean CO_2 concentration in Region1 more than that in Region2 by 0.86 ppmv decade^{-1} (Figure 8a). More than 1.3 ppmv decade^{-1} of the

regional differences in CO_2 concentration trends (Region2 minus Region1) exhibits in April and November, and less than 0.5 ppmv decade^{-1} of the regional differences are found in January and August. The annual mean trends of the regional differences mostly result from the increasing carbon emissions in eastern China (0.69 ppmv decade^{-1}; Figure 8b). The monthly variations of the regional differences are associated with wind circulation changes. For example, reduced westerly flow and northwesterly flow over the Korean Peninsula intensify the CO_2 concentration gradient from eastern China to Korea and increase the regional differences in April and November, respectively. However, the two regions shared similar seasonal patterns in CO_2 concentration trends. Even seasonally averaged trends of the regional differences are smaller during the growing season (-0.76 ppmv decade^{-1}) than they are during the non-growing season (-0.92 ppmv decade^{-1}). These results suggest that the change in atmospheric transport is not a main reason for the observed negative trends in ΔCO_2 during the growing season, distinct during the non-growing season.

Discussion

The best way to understand the terrestrial carbon cycle would be to use as many terrestrial carbon flux measurements as possible. However, the number of terrestrial carbon flux measurements is still limited in many parts of the globe (Schimel et al., 2015). Recent studies suggest the applicability of long-term measurements of atmospheric CO_2 concentrations to evaluate the regional terrestrial carbon flux changes (Commane et al., 2016; Jeong et al., 2018). This study assessed whether surface atmospheric CO_2 measurements can be used to understand the regional terrestrial carbon cycle in Korea. However, unlike the clean-air environment in Alaska where previous studies have been performed (Commane et al., 2016; Jeong et al., 2018), Korea is located at the center of the East Asia region where a rapid increase in anthropogenic carbon emissions have been reported over the recent decades (Global Carbon Project, 2018). The higher increasing trends of $CO_2^{YellowSea}$ and CO_2^{land} than that of the globally averaged CO_2 concentration (2.07 ppmv year^{-1}), derived from the NOAA/ESRL data (Dlugokencky & Tans, 2019), indicate that the influences of anthropogenic emissions on the spatiotemporal variations in CO_2 concentrations cannot be negligible over the region as highlighted in previous modeling (Ballav et al., 2012; Ballav et al., 2016) and observation studies (Umezawa et al., 2018).

The changes in regional land–surface carbon fluxes were estimated from the difference between $CO_2^{YellowSea}$ and CO_2^{land} in this study. Although our back-trajectory analysis showed that CO_2^{land} could represent the inflow of air masses at the AMY Station from the Korea Peninsula, we further checked the possible influences of air coming from the East Sea on the CO_2^{land} by comparing with CO_2 concentration at the ULD Station. On average, the CO_2 concentration at the ULD Station is lower than both CO_2^{land} and $CO_2^{YellowSea}$ by 2.2 and 3.1 ppm from January 2014 to October 2017 (Figure 9), respectively, because the ULD Station is located far from the CO_2 source regions. However, the seasonal variability of CO_2^{land} is greater than that of the CO_2 concentrations at the ULD Station and annual minimum value of the monthly CO_2^{land} is lower than that of the ULD Station in three of the past four years. For example, in 2014, the annual maximum and minimum values of monthly CO_2^{land} are 415.6 and 387.9 ppmv but those of the monthly ULD CO_2 concentration are 407.7 and 396.2 ppmv, respectively. In addition, averaged CO_2^{land} from May to September (400.3 ppmv) is lower than that of the ULD CO_2 concentration (403.9 ppmv) by 3.6 ppmv during the analysis period. These results indicate that the variations in CO_2^{land} are mainly attributed to the regional land–surface carbon fluxes rather than the air coming from the East Sea. Further, it is worth noting that Ballav et al. (2016) showed that the relatively high nocturnal CO_2 concentration over land was sometimes observed over the open ocean region the next day, mostly when wind blows from land to sea; thus, higher CO_2^{land} could be observed in those cases. However, our results show that clear seasonal variations in ΔCO_2 appear (Figure 3b) and CO_2^{land} has greater seasonal variability than that of both $CO_2^{YellowSea}$ (Figure 3a) and the ULD CO_2 concentrations (Figure 9). This indicates that ΔCO_2 can capture the regional land–surface carbon flux signals that are distinct from the surrounding area (the Yellow Sea and East Sea).

Based on the observed ΔCO_2, we found that regional land carbon uptake significantly increases relative to the surrounding ocean region during the growing season, as opposed to increase in land carbon emissions during the non-growing season. We first assumed that this was from an enhancement of terrestrial carbon uptake for the period and investigated the changes in vegetation and terrestrial carbon fluxes using available satellite datasets and model simulation results. Our analysis of the satellite datasets show that significant nationwide increasing trends in vegetation and its photosynthesis appear for the growing season. The results are in line with the

previous finding that the NDVI and vegetation production showed consistent long-term increasing trends in the region (Fang et al., 2014). The national forest inventory reporting that the forest volume of Korea increased by 142% from 1999 to 2015 is additional evidence for the increase in vegetation production (Korea Forest Service, 2018). Generally, major reasons for the vegetation greening are considered as fertilization effects of increasing ambient CO_2 and nitrogen deposition, warming-driven enhancement of photosynthesis, and lengthening of growing seasons (Jeong et al., 2013; Piao et al., 2015; Zhu et al., 2016). In addition to the environmental changes at a global scale, sustained national forest management campaigns during the last two decades seem to be another key driver. Contrasting NDVI trends between South Korea (Republic of Korea) and North Korea (Democratic People's Republic of Korea) are observed in Figure 4. While forest areas in South Korea have remained steady, massive deforestation has taken place in North Korea since the early 1990s (Cui et al., 2014; Engler, Teplyakov, & Adams, 2014). The different forest management history causes the vegetation browning trend in the southern area of North Korea despite the favorable environmental conditions for vegetation growth.

In accordance with the observed increasing trends of vegetation and its production, both TRENDY multi-model mean and CT2017 estimate the enhancement of terrestrial carbon uptake during the growing season, although the magnitudes differ by models. This study used the results of simulation S3, considering all changes to climate, CO_2, and land use, but found that there are little differences with the results of simulation S2, ignoring land use change (not shown here) despite Korean forests at least doubling in volume during the study period. It seems that the TRENDY models underestimate influences of land use change on terrestrial carbon fluxes. In addition, the globally averaged annual CO_2 concentration was equally prescribed in all regions in the TRENDY models. Considering that the increasing rate of atmospheric CO_2 concentration at the AMY Station is higher than that of the global mean value, the CO_2 fertilization effect could also be underestimated over the region. Thus, the process-based models (TRENDY) seem to estimate the increasing trends less than that of the inverse model constrained by CO_2 measurements data (CT2017). Although our CTM model simulations have relatively weaker responses to the estimated terrestrial carbon flux changes, they show that the observed ΔCO_2 decrease is mainly associated with the enhancement of terrestrial carbon uptake in Korea during the growing season rather than other factors (influences of other factors will be discussed in the

next paragraph). The results are consistent with previous studies estimating the strengthening of the carbon sink in Korean forests based on forest inventories (Pan et al., 2011; Jeong et al., 2013; Fang et al., 2014). Therefore, our findings provide evidence that atmospheric CO_2 measurements could be used to detect changes in the terrestrial carbon cycle at regional scales even where anthropogenic activities cannot be treated as minimal components.

This study suggests that enhanced terrestrial carbon uptake is a key process causing changes in temporal variations in ΔCO_2. However, ΔCO_2 variations can also be modulated by fossil fuel carbon emissions and atmospheric circulation changes. From the CTM model simulations, we checked all the potential influences of the factors. The model estimates that the increasing domestic fossil fuel carbon emissions do not cause notable seasonal differences in the CO_2 concentration trends in Korea. That is because seasonal variability of the carbon emissions trends is too small relative to the terrestrial carbon fluxes, which change sign in the growing season and non-growing season. Previous studies also show that the fossil fuel carbon emissions in main source regions have around 20% of seasonal variability of biospheric carbon fluxes over the tropics and northern middle latitude (Zhang, Gurney, Rayner, Baker, & Liu, 2016). Even with the small seasonal variability, our results show that the increasing carbon emissions in China, which are more than 40 times of those in Korea, has the potential to induce around 1 ppmv decade^{-1} increase of seasonal amplitude of atmospheric CO_2 over Korea. However, because the seasonal patterns of CO_2 concentration trends are similar around and in the Korean Peninsula, China's carbon emissions also seem to be a minor factor on the long-term trends in the seasonal variations of ΔCO_2. One thing to keep in mind is that the greater increasing rate of CO_2 concentrations in the Yellow Sea than the Korean Peninsula could alleviate the ΔCO_2 increase caused by increasing domestic carbon emissions. Readers need to be cautious when interpreting our results (decrease in annual ΔCO_2 trends does not mean that Korea becomes a net carbon sink). We also found that the atmospheric circulation changes have possibilities to induce unequal temporal changes in CO_2 concentrations over Korea. Our model simulation suggests, however, that there are no notable changes in atmospheric circulation patterns leading to the observed ΔCO_2 trend during the study period. In addition, although this study treated the anthropogenic emissions and atmospheric circulation as main drivers of transport changes, the enhancement of terrestrial carbon uptake in boreal forests, highlighted in previous studies (Graven et al., 2013; Welp et al., 2016), can also be

another driver. Welp et al. (2016) showed that significant increases in amplitude of biospheric CO_2 flux appear in boreal regions at 0.31% year^{-1} and in arctic regions at 0.85 % year^{-1} for 1985–2012 from inversion results. We evaluated the possible effect through a set of ideal model simulations with and without a 1% year^{-1} increase in seasonal amplitude of monthly terrestrial CO_2 fluxes in high-latitude regions ($> 45°N$) during the study period. The model estimated that the increasing biospheric carbon uptake increases the seasonal amplitude of CO_2 concentration around 1.5 ppmv decade^{-1} over Korea, but it also did not induce remarkable regional differences in the CO_2 concentration trends around the AMY station (not shown here).

The CTM simulations provide valuable evidence to support our hypothesis in company with independent satellite measurement and model simulation results; however, a practical limitation remains in our simulations. Our sensitivity tests of atmospheric CO_2 were conducted at a monthly scale instead of using hourly composite like the observations. Current CTMs are not able to represent locally measured hourly variations in CO_2 concentration due to the absence of validated hourly datasets representing land–surface carbon fluxes in Korea as well as most other regions (Zhu et al., 2014; Ballav et al., 2016), hence the difficulty of performing the exact same model configuration that matches our observation analysis. Nevertheless, in the case of atmospheric transportation effect, we checked whether our results are different when the sampling method is applied to the results of simulation E4 based on the assumption that the changes in air sources into the AMY Station have more effect than sub-monthly variations in land–surface carbon fluxes in remote areas. However, the difference between simulated CO_2^{land} and $CO_2^{YellowSea}$, derived by sampling simulated hourly CO_2 concentration at the station based on the MERRA2 wind data, shows seasonally uniform decreasing trends consistent with our findings based on the monthly averaged values (not shown here).

This study takes advantage of the long-term continuous CO_2 measurement at the AMY Station. In addition to the AMY Station, numerous surface stations are continuously measuring atmospheric CO_2 concentration over the globe and provide hourly data. Because many of these observation sites are located in coastal areas, our approach has potential to provide wide-area information. Even if the station is located far from the coast, we could retrieve signals of terrestrial

carbon exchange by considering physical characteristics of local wind circulation. For example, the Mauna Loa Observatory (MLO), located at a high altitude (3397 m) in the center of the Hawaiian Islands, observes CO_2 concentrations above the planetary boundary layer, but CO_2 concentrations are affected by the airflow blowing from lower altitudes to the site during a few hours after sunset (Sharma and Barnes, 2016). The difference in observed CO_2 concentration between the two periods could play the role of ΔCO_2 of this study. Additionally, local variations in land carbon flux within the continent could be detected by comparing atmospheric CO_2 data from adjacent observation sites (Sargent et al., 2018).

In summary, this study showed that the terrestrial carbon uptake has been enhanced resulting from the nationwide vegetation greening over Korea during the growing season for the past two decades based on multiple lines of evidence from atmospheric measurements, satellite observations, and model simulations. Additional surface observation sites have been operated in the mainland (Seoul) and test operations for long-term aircraft measurements across the Korean Peninsula have been conducted since 2018. Satellites like the Greenhouse gases Observing SATellite (GOSAT), Orbiting Carbon Observatory 2 (OCO-2), and TanSat also have measured a large spatial extent of column-averaged CO_2 concentrations. Inverse modeling using the added in situ, airborne, and satellite data would provide more reliable quantitative information on the enhanced terrestrial carbon uptake by using the relationship between our results (ΔCO_2) and the estimated biosphere flux in future studies (Commane et al., 2016). Atmospheric CO_2 measurements could generate the possibility for a better understanding of the terrestrial carbon cycle where ground-based observation is limited, therefore, sustained efforts to expand the observation network are required.

Data Accessibility Statement:

The atmospheric CO_2 measurement datasets at AMY and ULD Stations are available at https://gaw.kishou.go.jp/ and from Haeyoung Lee (leehy80@korea.kr) through e-mail request. The GIMMS NDVI is publicly available at https://ecocast.arc.nasa.gov/data/pub/gimms/3g.v1. MODIS NDVI and GPP are publicly available at https://lpdaac.usgs.gov/products/mod13c1v006 and https://lpdaac.usgs.gov/products/mod17a2hv006. The TRENDY model simulation results are available from Stephen Sitch (S.A.Sitch@exeter.ac.uk) or Pierre Friedlingstein (p.friedlingstein@exeter.ac.uk) through e-mail request. CarbonTracker results are publicly available at http://carbontracker.noaa.gov. ODIAC dataset are publicly available at doi:10.17595/20170411.001. The GEOS-Chem model simulation results that support the findings of this study are available from the corresponding author upon reasonable request.

References

Ballav, S., Patra, P. K., Sawa, Y., Matsueda, H., Adachi, A., Onogi, S., … De, U. K. (2016). Simulation of CO 2 concentrations at Tsukuba tall tower using WRF-CO 2 tracer transport model. *Journal of Earth System Science*, *125*(1), 47–64. https://doi.org/10.1007/s12040-015-0653-y

Ballav, S., Patra, P. K., Takigawa, M., Ghosh, S., De, U. K., Maksyutov, S., … Hashimoto, S. (2012). Simulation of CO2 concentration over East Asia using the regional transport model WRF-CO2. *Journal of the Meteorological Society of Japan. Ser. II*, *90*(6), 959–976. https://doi.org/10.2151/jmsj.2012-607

Barnes, E. A., Parazoo, N., Orbe, C., & Denning, A. S. (2016). Isentropic transport and the seasonal cycle amplitude of CO2. *Journal of Geophysical Research: Atmospheres*, *121*(13), 2016JD025109. https://doi.org/10.1002/2016JD025109

Bey, I., Jacob, D. J., Yantosca, R. M., Logan, J. A., Field, B. D., Fiore, A. M., … Schultz, M. G. (2001). Global modeling of tropospheric chemistry with assimilated meteorology: Model description and evaluation. *Journal of Geophysical Research: Atmospheres*, *106*(D19), 23073–23095. https://doi.org/10.1029/2001JD000807

Bruhwiler, L. M. P., Michalak, A. M., & Tans, P. P. (2011). Spatial and temporal resolution of carbon flux estimates for 1983–2002. *Biogeosciences*, *8*(5), 1309–1331. https://doi.org/10.5194/bg-8-1309-2011

Canadell, J. G., Ciais, P., Gurney, K., Quéré, C. L., Piao, S., Raupach, M. R., & Sabine, C. L. (2011). An international effort to quantify regional carbon fluxes. *Eos, Transactions American Geophysical Union*, *92*(10), 81–82. https://doi.org/10.1029/2011EO100001

Cho, C.-H., Kim, J.-S., & Yoo, H.-J. (2007). Atmospheric carbon dioxide variations at Korea GAW center from 1999 to 2006. *Asia-Pacific Journal of Atmospheric Sciences*, *43*(4), 359–365.

Choi, S.-D., Lee, K., & Chang, Y.-S. (2002). Large rate of uptake of atmospheric carbon dioxide by planted forest biomass in Korea. *Global Biogeochemical Cycles*, *16*(4), 1089. https://doi.org/10.1029/2002GB001914

Clark, D. B., Mercado, L. M., Sitch, S., Jones, C. D., Gedney, N., Best, M. J., … Cox, P. M. (2011). The Joint UK Land Environment Simulator (JULES), model description − Part 2: Carbon fluxes and vegetation dynamics. *Geoscientific Model Development*, *4*(3), 701–722.

https://doi.org/10.5194/gmd-4-701-2011

Commane, R., Lindaas, J., Benmergui, J., Luus, K. A., Chang, R. Y.-W., Daube, B. C., … Wofsy, S. C. (2017). Carbon dioxide sources from Alaska driven by increasing early winter respiration from Arctic tundra. *Proceedings of the National Academy of Sciences*, *114*(21), 5361–5366. https://doi.org/10.1073/pnas.1618567114

Cui, G., Lee, W.-K., Kim, D., Lee, E. J., Kwak, H., Choi, H.-A., … Jeon, S. (2014). Estimation of forest carbon budget from land cover change in South and North Korea between 1981 and 2010. *Journal of Plant Biology*, *57*(4), 225–238. https://doi.org/10.1007/s12374-014-0165-3

Didan, K. (2015). MOD13Q1 MODIS/Terra vegetation indices 16-day L3 global 250m SIN grid V006. *NASA EOSDIS Land Processes DAAC*.

Dlugokencky, E. & Tans, P. (2019). Trends in global CO_2, National Oceanic & Atmospheric Administration, Earth System Research Laboratory (NOAA/ESRL), available at http://www.esrl.noaa.gov/gmd/ccgg/trends.

Dragoni, D., Schmid, H. P., Wayson, C. A., Potter, H., Grimmond, C. S. B., & Randolph, J. C. (2011). Evidence of increased net ecosystem productivity associated with a longer vegetated season in a deciduous forest in south-central Indiana, USA. *Global Change Biology*, *17*(2), 886–897. https://doi.org/10.1111/j.1365-2486.2010.02281.x

Engler, R., Teplyakov, V., & Adams, J. M. (2014). An assessment of forest cover trends in South and North Korea, from 1980 to 2010. *Environmental Management*, *53*(1), 194–201. https://doi.org/10.1007/s00267-013-0201-y

Enting, I. G., & Mansbridge, J. V. (1989). Seasonal sources and sinks of atmospheric CO2 Direct inversion of filtered data. *Tellus B: Chemical and Physical Meteorology*, *41*(2), 111–126. https://doi.org/10.3402/tellusb.v41i2.15056

Fang, J., Guo, Z., Hu, H., Kato, T., Muraoka, H., & Son, Y. (2014). Forest biomass carbon sinks in East Asia, with special reference to the relative contributions of forest expansion and forest growth. *Global Change Biology*, *20*(6), 2019–2030. https://doi.org/10.1111/gcb.12512

Gelaro, R., McCarty, W., Suárez, M. J., Todling, R., Molod, A., Takacs, L., … Zhao, B. (2017). The Modern-Era Retrospective Analysis for Research and Applications, Version 2 (MERRA-2). *Journal of Climate*, *30*(14), 5419–5454. https://doi.org/10.1175/JCLI-D-16-0758.1

Global Carbon Project (2018). Supplemental data of Global Carbon Budget 2018 (Version 1.0) [2018 National Emissions v1.0], available at https://www.icos-cp.eu/GCP/2018.

Graven, H. D., Keeling, R. F., Piper, S. C., Patra, P. K., Stephens, B. B., Wofsy, S. C., … Bent, J. D. (2013). Enhanced seasonal exchange of CO2 by northern ecosystems since 1960. *Science*, *341*(6150), 1085–1089. https://doi.org/10.1126/science.1239207

Gurney, K. R., Law, R. M., Denning, A. S., Rayner, P. J., Baker, D., Bousquet, P., … Yuen, C.-W. (2003). TransCom 3 CO2 inversion intercomparison: 1. Annual mean control results and sensitivity to transport and prior flux information. *Tellus B: Chemical and Physical Meteorology*, *55*(2), 555–579. https://doi.org/10.3402/tellusb.v55i2.16728

Haverd, V., Smith, B., Nieradzik, L., Briggs, P. R., Woodgate, W., Trudinger, C. M., ... Cuntz, M. (2018). A new version of the CABLE land surface model (Subversion revision r4601) incorporating land use and land cover change, woody vegetation demography, and a novel optimisation-based approach to plant coordination of photosynthesis. *Geoscientific Model Development*, *11*(7), 2995-3026. https://doi.org/10.5194/gmd-11-2995-2018

Haverd, V., Raupach, M. R., Briggs, P. R., Canadell., J. G., Davis, S. J., Law, R. M., … Sherman, B. (2013). The Australian terrestrial carbon budget. *Biogeosciences*, *10*(2), 851–869. https://doi.org/10.5194/bg-10-851-2013

Hurtt, G. C., Chini, L. P., Frolking, S., Betts, R. A., Feddema, J., Fischer, G., ... Wang, Y. P. (2011). Harmonization of land-use scenarios for the period 1500–2100: 600 years of global gridded annual land-use transitions, wood harvest, and resulting secondary lands. *Climatic change*, *109*(1-2), 117. https://doi.org/10.1007/s10584-011-0153-2

IPCC (2014). Climate change 2014: *synthesis report. Contribution of Working Groups I, II and III to the fifth assessment report of the Intergovernmental Panel on Climate Change* (pp. 77-78) [Core Writing Team, R.K. Pachauri & L.A. Meyer (eds.)], IPCC, Geneva, Switzerland, 151 pp.

Ito, A., & Inatomi, M. (2012). Use of a process-based model for assessing the methane budgets of global terrestrial ecosystems and evaluation of uncertainty. *Biogeosciences*, *9*(2), 759–773. https://doi.org/10.5194/bg-9-759-2012

Jain, A. K., Meiyappan, P., Song, Y., & House, J. I. (2013). CO_2 emissions from land-use change affected more by nitrogen cycle, than by the choice of land-cover data. *Global Change*

Biology, *19*(9), 2893–2906. https://doi.org/10.1111/gcb.12207

Jeong, S.-J., Bloom, A. A., Schimel, D., Sweeney, C., Parazoo, N. C., Medvigy, D., … Miller, C. E. (2018). Accelerating rates of Arctic carbon cycling revealed by long-term atmospheric CO2 measurements. *Science Advances*, *4*(7), eaao1167. https://doi.org/10.1126/sciadv.aao1167

Jeong, S.-J., Ho, C.-H., Choi, S.-D., Kim, J., Lee, E.-J., & Gim, H.-J. (2013). Satellite data-based phenological evaluation of the nationwide reforestation of South Korea. *PLOS ONE*, *8*(3), e58900. https://doi.org/10.1371/journal.pone.0058900

Jeong, S.-J., Ho, C.-H., & Jeong, J.-H. (2009). Increase in vegetation greenness and decrease in springtime warming over east Asia. *Geophysical Research Letters*, *36*(2), L02710. https://doi.org/10.1029/2008GL036583

Joos, F., & Spahni, R. (2008). Rates of change in natural and anthropogenic radiative forcing over the past 20,000 years. *Proceedings of the National Academy of Sciences*, *105*(5), 1425–1430. https://doi.org/10.1073/pnas.0707386105

Keenan, T. F., Gray, J., Friedl, M. A., Toomey, M., Bohrer, G., Hollinger, D. Y., … Richardson, A. D. (2014). Net carbon uptake has increased through warming-induced changes in temperate forest phenology. *Nature Climate Change*, *4*(7), 598–604. https://doi.org/10.1038/nclimate2253

Korea Forest Service (2018) Statistical yearbook of forest. Korea Forest Service, Seoul, Republic of Korea.

Krinner, G., Viovy, N., Noblet-Ducoudré, N. de, Ogée, J., Polcher, J., Friedlingstein, P., … Prentice, I. C. (2005). A dynamic global vegetation model for studies of the coupled atmosphere-biosphere system. *Global Biogeochemical Cycles*, *19*(1). https://doi.org/10.1029/2003GB002199

Le Quéré, C., Andrew, R. M., Friedlingstein, P., Sitch, S., Hauck, J., Pongratz, J., ... & Zheng, B. (2018). Global carbon budget 2018. *Earth System Science Data (Online)*, *10*(4). https://doi.org/10.5194/essd-10-2141-2018

Lee, H., Han, S.-O., Ryoo, S.-B., Lee, J.-S., & Lee, G.-W. (2019). The measurement of atmospheric CO_2 at KMA GAW regional stations, its characteristics, and comparisons with

other East Asian sites. *Atmospheric Chemistry and Physics*, *19*(4), 2149–2163. https://doi.org/10.5194/acp-19-2149-2019

Lee, J.-Y., Kwon, M., Yun, K.-S., Min, S.-K., Park, I.-H., Ham, Y.-G., … Yoon, J.-H. (2017). The long-term variability of Changma in the East Asian summer monsoon system: A review and revisit. *Asia-Pacific Journal of Atmospheric Sciences*, *53*(2), 257–272. https://doi.org/10.1007/s13143-017-0032-5

Lee, J., Yoon, T. K., Han, S., Kim, S., Yi, M. J., Park, G. S., … Son, Y. (2014). Estimating the carbon dynamics of South Korean forests from 1954 to 2012. *Biogeosciences*, *11*(17), 4637–4650. https://doi.org/10.5194/bg-11-4637-2014

Li, X., Yi, M. J., Son, Y., Jin, G., & Han, S. S. (2010). Forest biomass carbon accumulation in Korea from 1954 to 2007. *Scandinavian Journal of Forest Research*, *25*(6), 554–563. https://doi.org/10.1080/02827581.2010.524892

Liu, J., Bowman, K. W., Lee, M., Henze, D. K., Bousserez, N., Brix, H., … Nassar, R. (2014). Carbon monitoring system flux estimation and attribution: impact of ACOS-GOSAT XCO2 sampling on the inference of terrestrial biospheric sources and sinks. *Tellus B: Chemical and Physical Meteorology*, *66*(1), 22486. https://doi.org/10.3402/tellusb.v66.22486

Min, S.-K., Zhang, X., Zwiers, F. W., & Hegerl, G. C. (2011). Human contribution to more-intense precipitation extremes. *Nature*, *470*(7334), 378–381. https://doi.org/10.1038/nature09763

MODIS Land Team (2018). Status for: Vegetation Indices (MOD13), online: https://landval.gsfc.nasa.gov/ProductStatus.php?ProductID=MOD13

Nassar, R., Napier-Linton, L., Gurney, K. R., Andres, R. J., Oda, T., Vogel, F. R., & Deng, F. (2013). Improving the temporal and spatial distribution of CO2 emissions from global fossil fuel emission data sets. *Journal of Geophysical Research: Atmospheres*, *118*(2), 917–933. https://doi.org/10.1029/2012JD018196

Nassar, R., Jones, D. B. A., Kulawik, S. S., Worden, J. R., Bowman, K. W., Andres, R. J., … Worthy, D. E. (2011). Inverse modeling of CO_2 sources and sinks using satellite observations of CO_2 from TES and surface flask measurements. *Atmospheric Chemistry and Physics*, *11*(12), 6029–6047. https://doi.org/10.5194/acp-11-6029-2011

Oda, T., & Maksyutov, S. (2011). A very high-resolution (1 km×1 km) global fossil fuel CO_2 emission inventory derived using a point source database and satellite observations of nighttime lights. *Atmos. Chem. Phys.*, *11*(2), 543–556. https://doi.org/10.5194/acp-11-543-2011

Oleson, K. W., Lawrence, D. M., Gordon, B., Flanner, M. G., Kluzek, E., Peter, J., …Heald, C. L. (2013). Technical description of version 4.5 of the Community Land Model (CLM), NCAR Technical Note NCAR/TN-503+STR. 420 pp.

Pan, Y., Birdsey, R. A., Fang, J., Houghton, R., Kauppi, P. E., Kurz, W. A., … Hayes, D. (2011). A large and persistent carbon sink in the world's forests. *Science*, *333*(6045), 988–993. https://doi.org/10.1126/science.1201609

Parazoo, N. C., Commane, R., Wofsy, S. C., Koven, C. D., Sweeney, C., Lawrence, D. M., … Miller, C. E. (2016). Detecting regional patterns of changing CO_2 flux in Alaska. *Proceedings of the National Academy of Sciences*, *113*(28), 7733–7738. https://doi.org/10.1073/pnas.1601085113

Patra, P. K., Canadell, J. G., Houghton, R. A., Piao, S. L., Oh, N.-H., Ciais, P., … Lasco, R. (2013). The carbon budget of South Asia. *Biogeosciences*, *10*(1), 513–527.

Patra, P., Law, R. M., Peters, W., Rödenbeck, C., Takigawa, M., Aulagnier, C., ... & Bruhwiler, L. (2008). TransCom model simulations of hourly atmospheric CO_2: Analysis of synoptic-scale variations for the period 2002–2003. *Global Biogeochemical Cycles*, *22*(4). https://doi.org/10.1029/2007GB003081

Peters, W., Jacobson, A. R., Sweeney, C., Andrews, A. E., Conway, T. J., Masarie, K., … Tans, P. P. (2007). An atmospheric perspective on North American carbon dioxide exchange: CarbonTracker. *Proceedings of the National Academy of Sciences*, *104*(48), 18925–18930. https://doi.org/10.1073/pnas.0708986104

Peylin, P., Law, R. M., Gurney, K. R., Chevallier, F., Jacobson, A. R., Maki, T., … Zhang, X. (2013). Global atmospheric carbon budget: Results from an ensemble of atmospheric CO_2 inversions. *Biogeosciences*, *10*, 6699–6720. https://doi.org/10.5194/bg-10-6699-2013

Piao, S., Yin, G., Tan, J., Cheng, L., Huang, M., Li, Y., … Wang, Y. (2015). Detection and attribution of vegetation greening trend in China over the last 30 years. *Global Change Biology*, *21*(4), 1601–1609. https://doi.org/10.1111/gcb.12795

Piao, S., Sitch, S., Ciais, P., Friedlingstein, P., Peylin, P., Wang, X., … Zeng, N. (2013). Evaluation of terrestrial carbon cycle models for their response to climate variability and to CO2 trends. *Global Change Biology*, *19*(7), 2117–2132. https://doi.org/10.1111/gcb.12187

Piao, S. L., Ito, A., Li, S. G., Huang, Y., Ciais, P., Wang, X. H., … Zhu, B. (2012). The carbon budget of terrestrial ecosystems in East Asia over the last two decades. *Biogeosciences*, *9*(9), 3571–3586. https://doi.org/10.5194/bg-9-3571-2012

Piao, S., Ciais, P., Lomas, M., Beer, C., Liu, H., Fang, J., … Woodward, I. (2011). Contribution of climate change and rising CO2 to terrestrial carbon balance in East Asia: A multi-model analysis. *Global and Planetary Change*, *75*(3), 133–142. https://doi.org/10.1016/j.gloplacha.2010.10.014

Piao, S., Ciais, P., Friedlingstein, P., Peylin, P., Reichstein, M., Luyssaert, S., … Vesala, T. (2008). Net carbon dioxide losses of northern ecosystems in response to autumn warming. *Nature*, *451*(7174), 49–52. https://doi.org/10.1038/nature06444

Pinzon, J. E., & Tucker, C. J. (2014). A non-stationary 1981–2012 AVHRR NDVI3g time series. *Remote Sensing*, *6*(8), 6929–6960. https://doi.org/10.3390/rs6086929

Randerson, J. T., Van Der Werf, G. R., Giglio, L., Collatz, G. J., & Kasibhatla, P. S. (2018). Global Fire Emissions Database, Version 4, (GFEDv4). ORNL DAAC, Oak Ridge, Tennessee, USA, available at https://doi.org/10.3334/ORNLDAAC/1293

Running, S. W., & Zhao, M. (2015). Daily GPP and annual NPP (MOD17A2/A3) products NASA Earth Observing System MODIS land algorithm. *MOD17 User's Guide*, *2015*.

Sargent, M., Barrera, Y., Nehrkorn, T., Hutyra, L. R., Gately, C. K., Jones, T., … Wofsy, S. C. (2018). Anthropogenic and biogenic CO2 fluxes in the Boston urban region. *Proceedings of the National Academy of Sciences*, *115*(29), 7491–7496. https://doi.org/10.1073/pnas.1803715115

Schimel, D., Pavlick, R., Fisher, J. B., Asner, G. P., Saatchi, S., Townsend, P., … Cox, P. (2015). Observing terrestrial ecosystems and the carbon cycle from space. *Global Change Biology*, *21*(5), 1762–1776. https://doi.org/10.1111/gcb.12822

Seneviratne, S. I., Donat, M. G., Pitman, A. J., Knutti, R., & Wilby, R. L. (2016). Allowable CO2 emissions based on regional and impact-related climate targets. *Nature*, *529*(7587), 477–483. https://doi.org/10.1038/nature16542

Sharma, N. C. P., & Barnes, J. E. (2016). Boundary layer characteristics over a high altitude station, Mauna Loa Observatory. *Aerosol and Air Quality Research*, *16*(3), 729–737. https://doi.org/10.4209/aaqr.2015.05.0347

Simone, N. W., Stettler, M. E. J., & Barrett, S. R. H. (2013). Rapid estimation of global civil aviation emissions with uncertainty quantification. *Transportation Research Part D: Transport and Environment*, *25*, 33–41. https://doi.org/10.1016/j.trd.2013.07.001

Sitch, S., Friedlingstein, P., Gruber, N., Jones, S. D., Murray-Tortarolo, G., Ahlström, A., … Myneni, R. (2015). Recent trends and drivers of regional sources and sinks of carbon dioxide. *Biogeosciences*, *12*(3), 653–679. https://doi.org/10.5194/bg-12-653-2015

Sitch, S., Smith, B., Prentice, I. C., Arneth, A., Bondeau, A., Cramer, W., … Venevsky, S. (2003). Evaluation of ecosystem dynamics, plant geography and terrestrial carbon cycling in the LPJ dynamic global vegetation model. *Global Change Biology*, *9*(2), 161–185. https://doi.org/10.1046/j.1365-2486.2003.00569.x

Stein, A. F., Draxler, R. R., Rolph, G. D., Stunder, B. J. B., Cohen, M. D., & Ngan, F. (2015). NOAA's HYSPLIT atmospheric transport and dispersion modeling system. *Bulletin of the American Meteorological Society*, *96*(12), 2059–2077. https://doi.org/10.1175/BAMS-D-14-00110.1

Stocker, B. D., Feissli, F., Strassmann, K. M., Spahni, R., & Joos, F. (2014). Past and future carbon fluxes from land use change, shifting cultivation and wood harvest. *Tellus B: Chemical and Physical Meteorology*, *66*(1), 23188. https://doi.org/10.3402/tellusb.v66.23188

Sweeney, C., Dlugokencky, E., Miller, C. E., Wofsy, S., Karion, A., Dinardo, S., … Tans, P. (2016). No significant increase in long-term CH4 emissions on North Slope of Alaska despite significant increase in air temperature. *Geophysical Research Letters*, *43*(12), 2016GL069292. https://doi.org/10.1002/2016GL069292

Takahashi, T., Sutherland, S. C., Wanninkhof, R., Sweeney, C., Feely, R. A., Chipman, D. W., … de Baar, H. J. W. (2009). Climatological mean and decadal change in surface ocean pCO2,

and net sea–air CO2 flux over the global oceans. *Deep Sea Research Part II: Topical Studies in Oceanography*, *56*(8), 554–577. https://doi.org/10.1016/j.dsr2.2008.12.009

Thompson, R. L., Patra, P. K., Chevallier, F., Maksyutov, S., Law, R. M., Ziehn, T., … Ciais, P. (2016). Top–down assessment of the Asian carbon budget since the mid 1990s. *Nature Communications*, *7*, 10724. https://doi.org/10.1038/ncomms10724

Thoning, K. W., Tans, P. P., & Komhyr, W. D. (1989). Atmospheric carbon dioxide at Mauna Loa Observatory: 2. Analysis of the NOAA GMCC data, 1974–1985. *Journal of Geophysical Research: Atmospheres*, *94*(D6), 8549–8565. https://doi.org/10.1029/JD094iD06p08549

Tian, H., Chen, G., Lu, C., Xu, X., Hayes, D. J., Ren, W., … Wofsy, S. C. (2015). North American terrestrial CO2 uptake largely offset by CH4 and N2O emissions: toward a full accounting of the greenhouse gas budget. *Climatic Change*, *129*(3), 413–426. https://doi.org/10.1007/s10584-014-1072-9

Umezawa, T., Matsueda, H., Sawa, Y., Niwa, Y., Machida, T., & Zhou, L. (2018). Seasonal evaluation of tropospheric CO2 over the Asia-Pacific region observed by the CONTRAIL commercial airliner measurements. *Atmospheric Chemistry and Physics Discussions*, 1–28. https://doi.org/10.5194/acp-2018-519

Wang, Y. X., McElroy, M. B., Jacob, D. J., & Yantosca, R. M. (2004). A nested grid formulation for chemical transport over Asia: Applications to CO. *Journal of Geophysical Research: Atmospheres*, *109*(D22). https://doi.org/10.1029/2004JD005237

Welp, L. R., Patra, P. K., Rödenbeck, C., Nemani, R., Bi, J., Piper, S. C., & Keeling, R. F. (2016). Increasing summer net CO_2 uptake in high northern ecosystems inferred from atmospheric inversions and comparisons to remote-sensing NDVI. *Atmospheric Chemistry and Physics*, *16*(14), 9047–9066. https://doi.org/10.5194/acp-16-9047-2016

World Bank. (2018). GDP per capita (current US$). Washington, D.C., The World Bank Online: https://data.worldbank.org/indicator/NY.GDP.MKTP.CD?locations=KR

Yevich, R., & Logan, J. A. (2003). An assessment of biofuel use and burning of agricultural waste in the developing world. *Global Biogeochemical Cycles*, *17*(4), n/a-n/a. https://doi.org/10.1029/2002GB001952

Yue, X., Unger, N., & Zheng, Y. (2015). Distinguishing the drivers of trends in land carbon fluxes and plant volatile emissions over the past 3 decades. *Atmos. Chem. Phys.*, *15*(20), 11931–11948. https://doi.org/10.5194/acp-15-11931-2015

Yun, S. J., & Chun, J. (2018). Long-term ecological research on Korean forest ecosystems: the current status and challenges. *Ecological Research*, *33*(6), 1289–1302. https://doi.org/10.1007/s11284-018-1645-6

Zaehle, S., Friedlingstein, P., & Friend, A. D. (2010). Terrestrial nitrogen feedbacks may accelerate future climate change. *Geophysical Research Letters*, *37*(1). https://doi.org/10.1029/2009GL041345

Zeng, N., Mariotti, A., & Wetzel, P. (2005). Terrestrial mechanisms of interannual CO_2 variability. *Global Biogeochemical Cycles*, *19*(1). https://doi.org/10.1029/2004GB002273

Zhang, Y., Song, C., Band, L. E., Sun, G., & Li, J. (2017). Reanalysis of global terrestrial vegetation trends from MODIS products: Browning or greening? *Remote Sensing of Environment*, *191*, 145–155. https://doi.org/10.1016/j.rse.2016.12.018

Zhang, X., Gurney, K. R., Rayner, P., Baker, D., & Liu, Y.-P. (2016). Sensitivity of simulated CO_2 concentration to sub-annual variations in fossil fuel CO_2 emissions. *Atmos. Chem. Phys.*, *16*(4), 1907–1918. https://doi.org/10.5194/acp-16-1907-2016

Zhu, Z., Piao, S., Myneni, R. B., Huang, M., Zeng, Z., Canadell, J. G., … Zeng, N. (2016). Greening of the Earth and its drivers. *Nature Climate Change*, *6*(8), 791–795. https://doi.org/10.1038/nclimate3004

Zhu, Z., Pawson, S., Collatz, G. J., Gregg, W. W., Kawa, S. R., Baker, D., & Ott, L. (2014). Sensitivity of CO_2 Simulation in a GCM to the Convective Transport Algorithms. *NASA technical reports server*.

Tables

Table 1 A set of model simulations to estimate the influences of changes in regional land−surface carbon fluxes and atmospheric transport on atmospheric CO_2 over the Republic of Korea for the period 2000–2016.

Simulations	Descriptions	
	Terrestrial carbon flux	Fossil Fuel carbon emissions
E1	**T**	**T**
E2	Korea **FIX**	**T**
E3	**T**	Korea **FIX**
E4	Korea **FIX**	Korea **FIX**
E5	**T**	Eastern China **FIX**

T: All transient variables are used.

FIX: Fluxes in 2000 are repeatedly prescribed over the region.

Figure 1 Locations of Anmyeondo (AMY; open box) and Ulleungdo Observatories (ULD; open circle) and positions of the Yellow Sea and land sectors. The Yellow Sea sector is defined as the region where wind blows from 225–315° and the land sector is defined as the region where wind blows from 45–135° with respect to the AMY Station. The inset figure shows the location of the Republic of Korea over East Asia.

Figure 2 Density plots for 48-h trajectories terminating at the AMY Station for wind from **(a)** the Yellow Sea sector and **(b)** the land sector for the period 1999–2017. Solid line represents the median trajectory. Markers on the trajectories represent the position of air masses at 6-hour intervals. Upper-right numbers of each plot signify the ratio of air masses that came into the domain (boxed area; 35.5–37.5°N, 125.3–127.3°E) from the ocean (land) side among the total air mass of wind from the Yellow Sea sector (land sector).

Figure 3 Variations of **(a)** monthly CO_2 concentrations for wind from the Yellow Sea sector ($CO_2^{YellowSea}$; blue line) and land sector (CO_2^{land}; red line) for the period 1999–2017. **(b)** Annually averaged monthly ΔCO_2 during the entire study period (black thick line), the first eight years (1999–2006; red bar), and the last eight years (2010–2017; blue bar). Error bar shows the monthly standard derivation of ΔCO_2. **(c)** Annual trends of monthly ΔCO_2 for the same period. The asterisk and cross indicate statistical significance at the 95% and 90% confidence level, respectively.

Figure 4 Spatial distributions of climatology and annual trend in averaged **(a)** GIMMS and **(b)** MODIS normalized difference vegetation index (NDVI) during the growing season (May through October) over the period 1999–2015 and 2000–2017, respectively. The stippled areas represent statistically significant correlations ($p < 0.05$). **(c)** Same as (b) but for accumulated gross primary production (GPP) from MODIS.
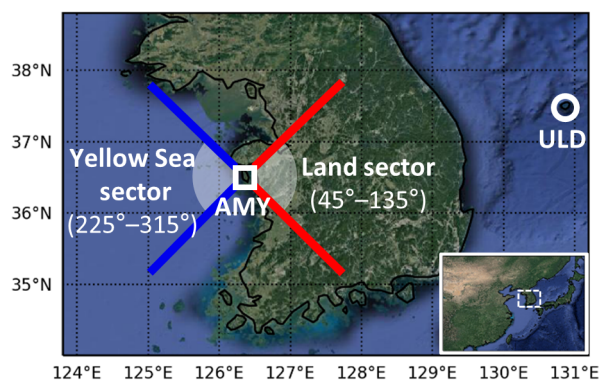
Figure 5 Area-averaged climatology and annual trend in monthly **(a)** gross primary production (GPP), **(b)** total respiration (i.e. autotrophic respiration + heterotrophic respiration), and **(c)** net biome production (NBP) over the Republic of Korea simulated from TRENDY models (black line) over the period 2000–2016. The shading denotes one inter-model standard deviation range of each month. The dotted lines represent the monthly minimum and maximum trends of the estimated carbon fluxes from TRENDY models. Blue and red lines indicate GPP from MODIS and biosphere carbon flux from CT2017, respectively.

Figure 6 Area-averaged changes in annual trends in monthly CO_2 concentrations due to **(a)** regional terrestrial carbon fluxes (red solid line: CT2017; simulation E1 minus simulation E3, black solid and dotted lines: average, maximum, and minimum of TRENDY models' estimates; simulations T2, T3, and T4 minus simulation T1, respectively) and **(b)** fossil fuel carbon emissions (i.e., simulation E1 minus simulation E2) at the Republic of Korea for the period 2000–2016.
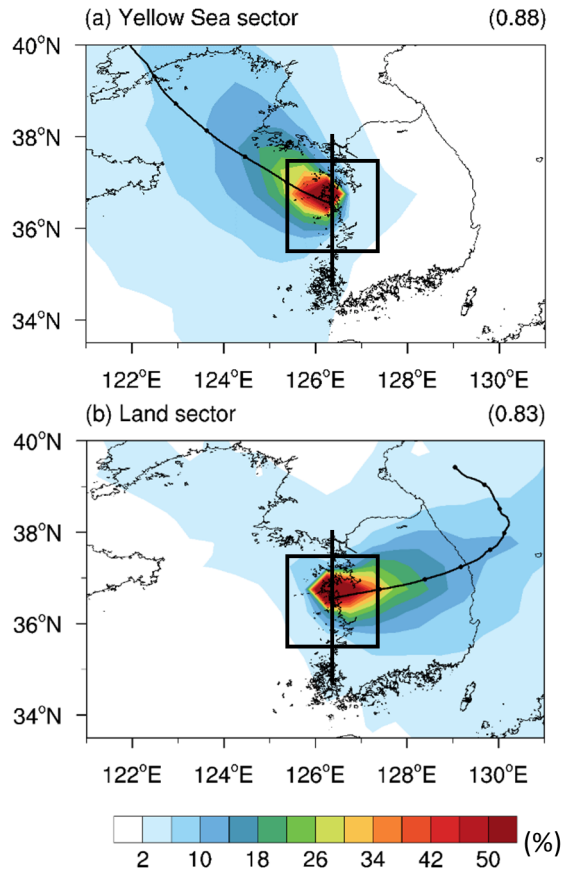
Figure 7 Spatial distributions of changes in simulated annual mean CO_2 concentration trends due to **(a)** atmospheric transport (simulation E4) and **(b)** China's fossil fuel carbon emissions (simulation E1 minus simulation E5) for the period 2000–2016.

Figure 8 Area-averaged changes in simulated monthly CO_2 concentration trends due to **(a)** atmospheric transport (i.e. simulation E4) and **(b)** China's fossil fuel carbon emissions (i.e., simulation E1 minus simulation E5) at the Region1 (35–38°N, 124.3–126.3°E), Region2 (35–38°N, 126.3–128.3°E), and difference between them for the period 2000–2016.
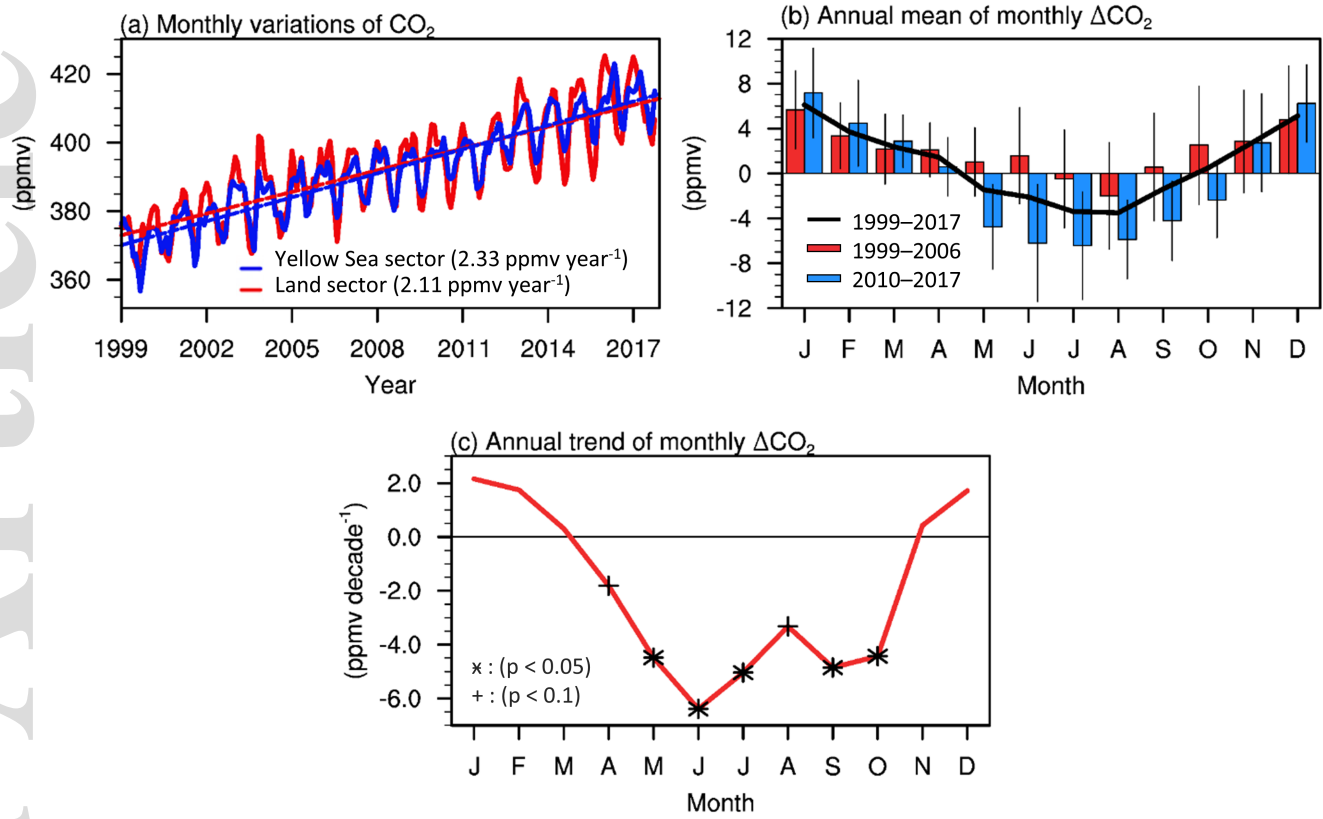
Figure 9 Variations of monthly CO_2 concentration at Ulleungdo Station (ULD; black line) and CO_2 concentrations for wind from the Yellow Sea sector ($CO_2^{YellowSea}$; blue line) and land sector (CO_2^{land}; red line) at Anmyeondo Station (AMY) from January 2014 to October 2017. The shading denotes two standard deviation range of CO_2 concentration of each month**.**

gcb_15061_f1.png

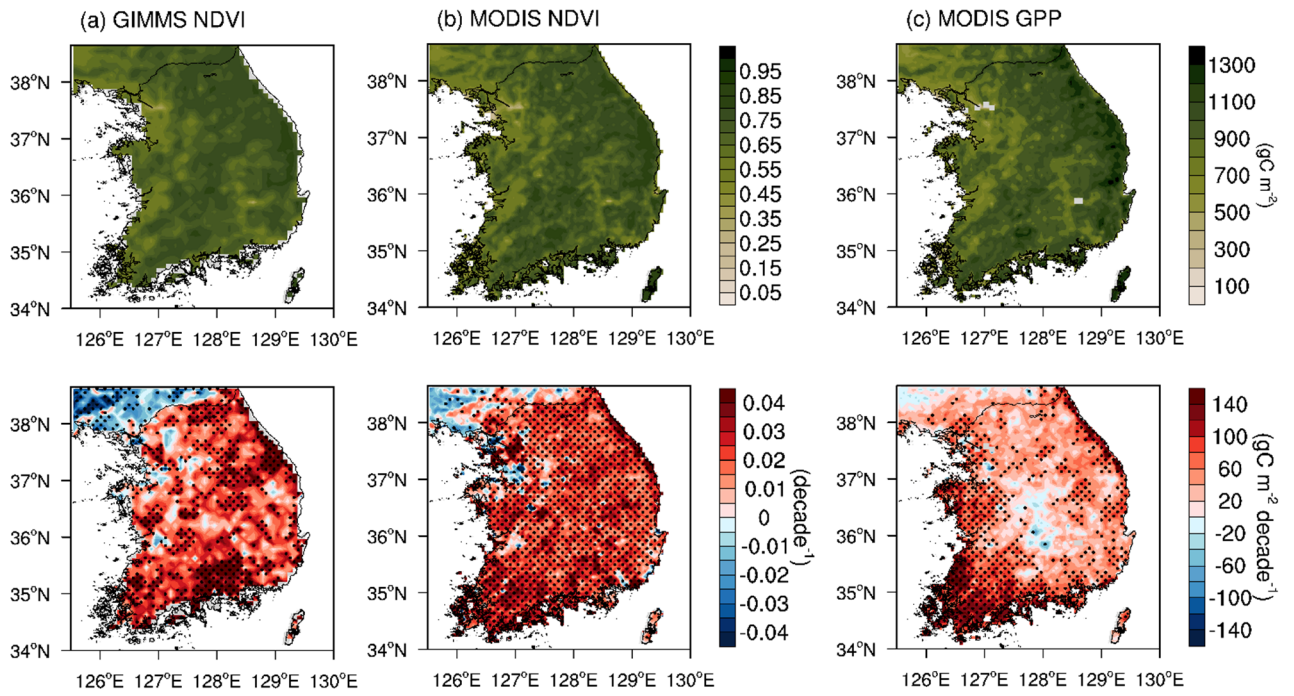(a) Yellow Sea sector (0.88)

(b) Land sector (0.83)

(%)

gcb_15061_f2.png

(a) Monthly variations of CO_2

Yellow Sea sector (2.33 ppmv year^{-1})
Land sector (2.11 ppmv year^{-1})

(b) Annual mean of monthly ΔCO_2

1999–2017
1999–2006
2010–2017

(c) Annual trend of monthly ΔCO_2

$*$: ($p < 0.05$)
$+$: ($p < 0.1$)

gcb_15061_f3.png

gcb_15061_f4.png

gcb_15061_f5.png

(a) Biospheric carbon fluxes

(b) Fossil fuel carbon emissions
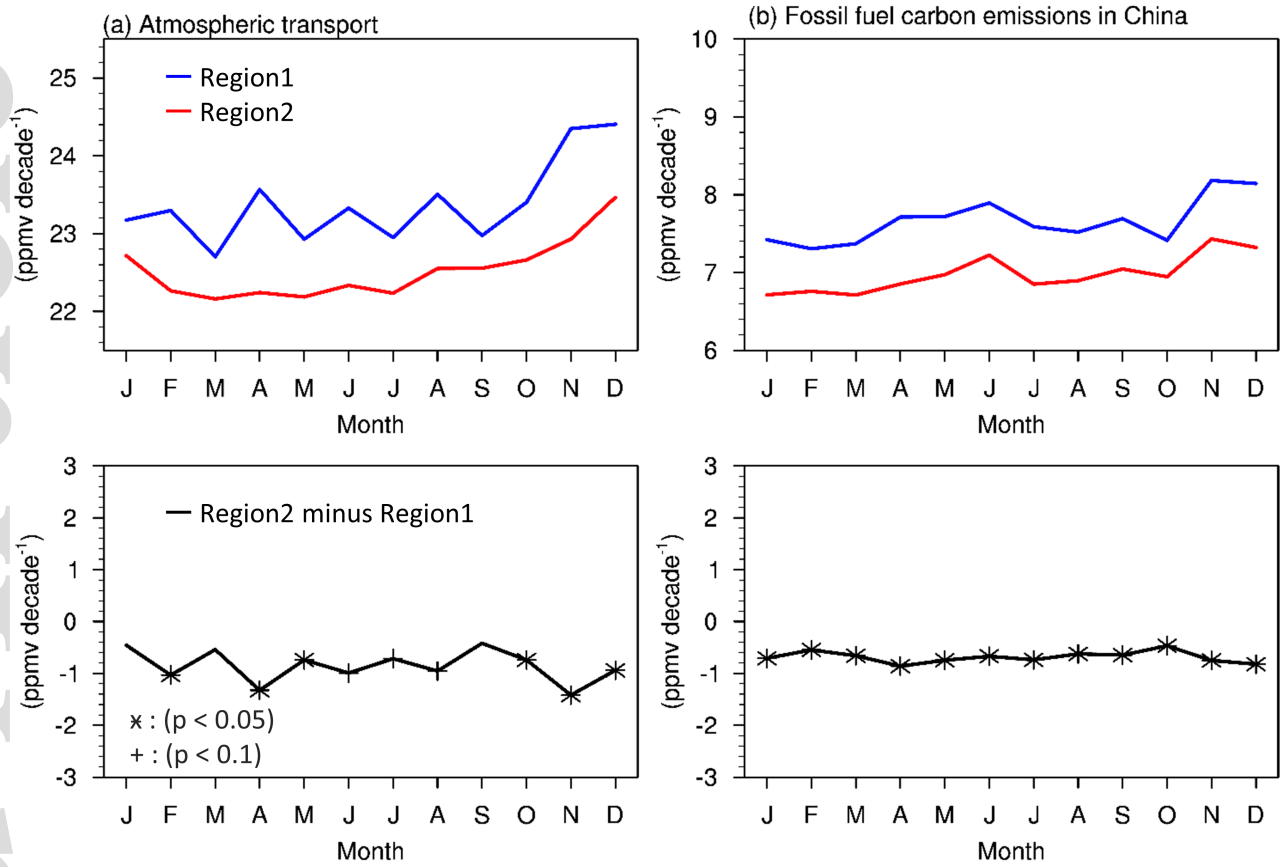
— TRENDY
— CT2017
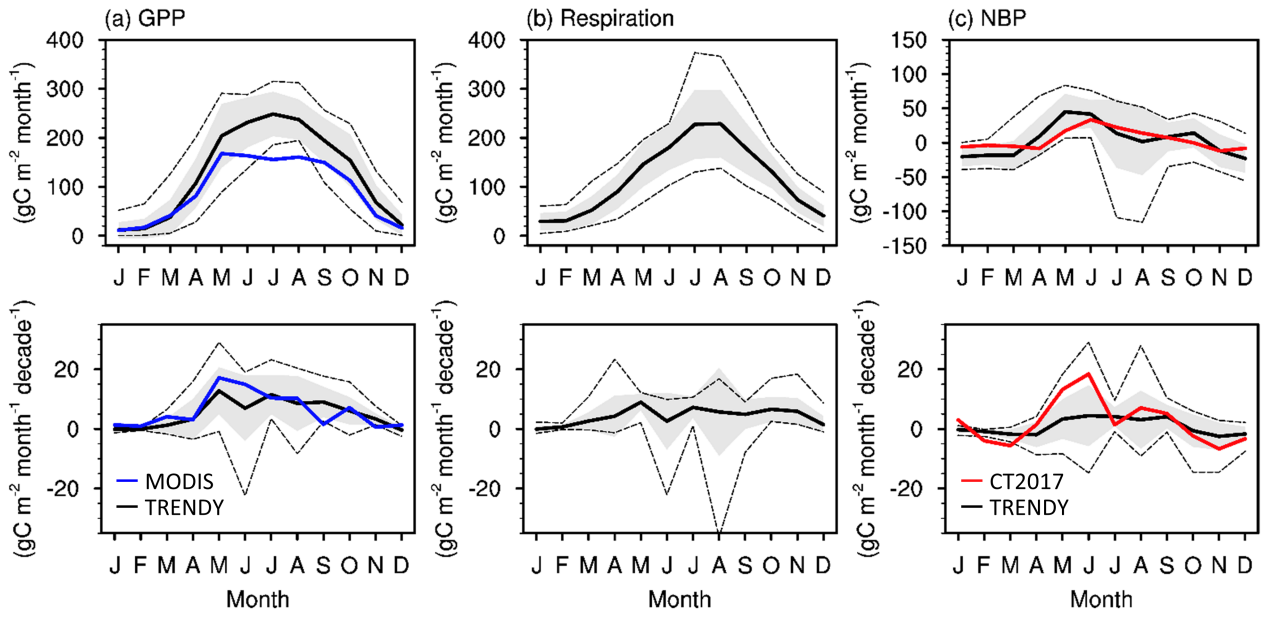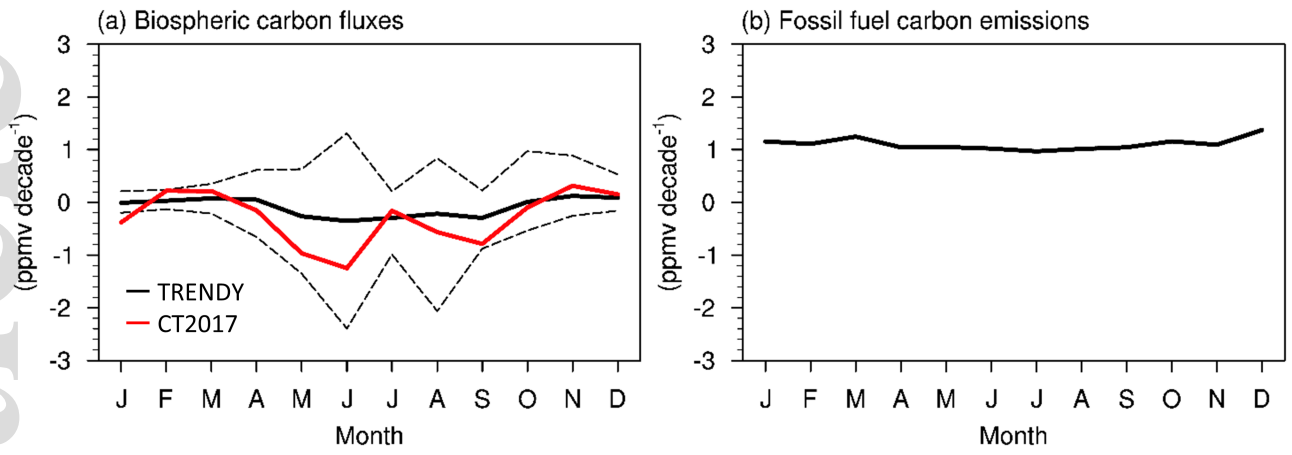
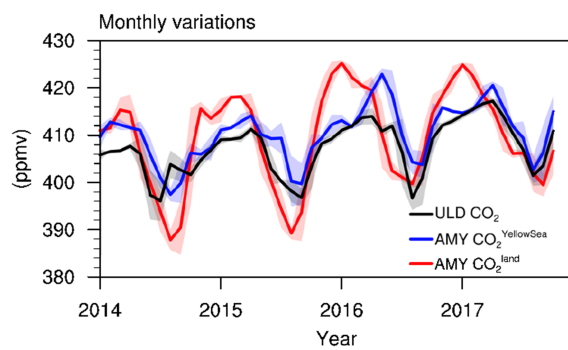gcb_15061_f6.png
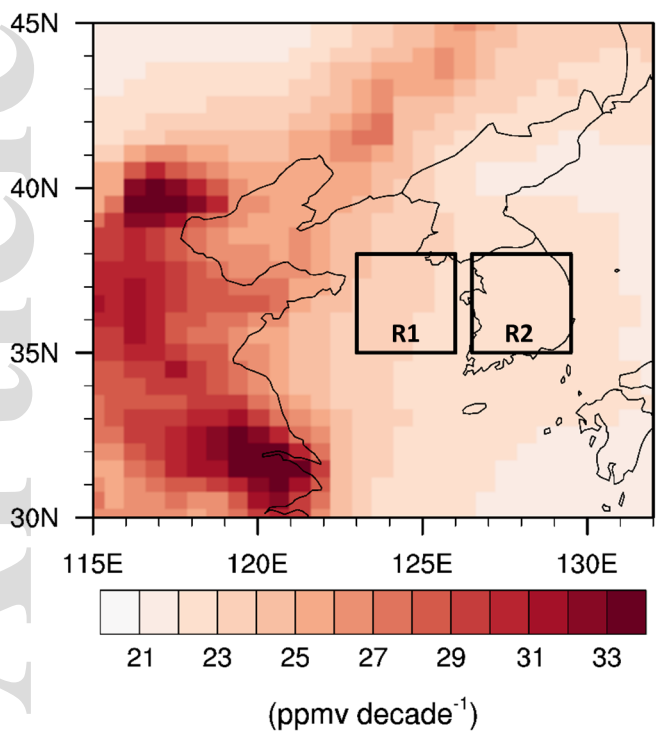
(a) Atmospheric transport   (b) Fossil fuel carbon emissions in China
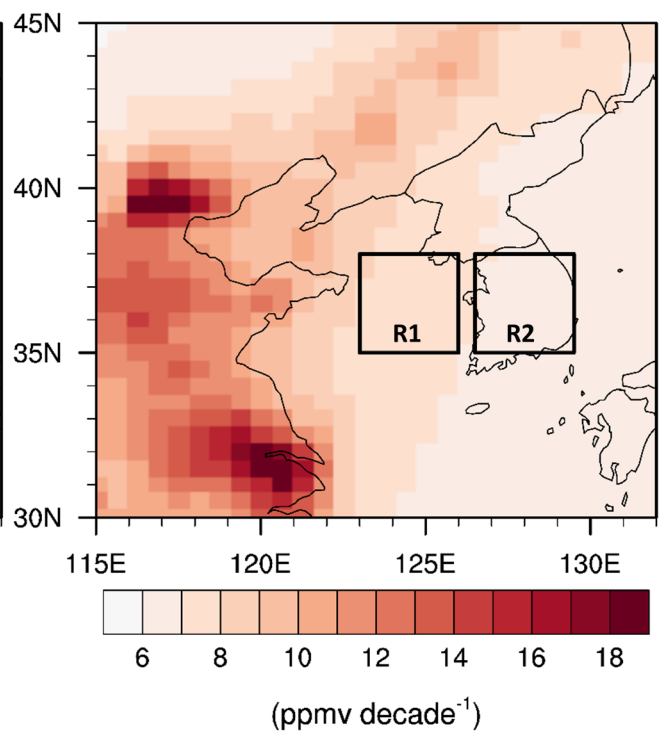
gcb_15061_f7.png

gcb_15061_f8.png

gcb_15061_f9.png